



Cite this: *Chem. Commun.*, 2015, 51, 7317

Received 10th February 2015,
Accepted 23rd March 2015

DOI: 10.1039/c5cc01254f

www.rsc.org/chemcomm

Magnetocaloric effect and thermal conductivity of $\text{Gd}(\text{OH})_3$ and $\text{Gd}_2\text{O}(\text{OH})_4(\text{H}_2\text{O})_2$ †

Yan Yang, Qian-Chong Zhang, Yin-Yin Pan, La-Sheng Long* and Lan-Sun Zheng

Magnetocaloric effect (MCE) and thermal conductivity of two gadolinium hydroxides, $\text{Gd}(\text{OH})_3$ (1) and $\text{Gd}_2\text{O}(\text{OH})_4(\text{H}_2\text{O})_2$ (2), are investigated. Magnetic studies indicate that both 1 and 2 exhibit antiferromagnetic interaction, and the MCE values for 1 and 2 at 2 K and $\Delta H = 7$ T are $62.00 \text{ J kg}^{-1} \text{ K}^{-1}$ and $59.09 \text{ J kg}^{-1} \text{ K}^{-1}$, respectively. Investigation of their thermal conductivity reveals that the thermal conductivity for 1 is significantly better than that for 2.

Since the discovery of the magnetocaloric effect (MCE) by Warburg in 1881,¹ magnetic refrigeration, a cooling technology based on the MCE,² has attracted much interest in the field of magnetic materials,³ due to its environmental friendliness and energy efficiency.^{3b} Among different types of magnetic materials, metal clusters and coordination polymers are especially notable. On one hand, their structural diversity and controllability facilitate us to adjust the magnetic interaction between the metal ions, leading to an MCE significantly larger than that of lanthanide alloys and magnetic nanoparticles;^{4,5} On the other hand, using these kinds of magnetic materials as magnetic reagents can achieve ultra-low temperature,^{3d} due to their magnetic phase transition often occurring at extremely low temperature.⁴⁻⁶ In the past few decades, a lot of metal clusters and coordination polymers, such as $\{\text{Mn}_{12}\}$,⁷ $\{\text{Fe}_8\}$,⁸ $\{\text{Mn}_4\text{Gd}_4\}$,⁹ $\{\text{Gd}_{36}\text{Ni}_{12}\}$,¹⁰ $\{\text{Gd}_{42}\text{Co}_{10}\}$,¹¹ $\{\text{Gd}_2\}$,¹² $[\text{Gd}(\text{HCOO})_3]_n$,⁴ $[\text{Gd}(\text{OH})\text{CO}_3]_n$,⁵ $[\text{Gd}_2(\text{OH})_2(\text{suc})_2(\text{H}_2\text{O})]_n \cdot 2n\text{H}_2\text{O}$ ¹³ and $[\text{Gd}_6(\text{OH})_8(\text{suc})_5(\text{H}_2\text{O})_2]_n \cdot 4n\text{H}_2\text{O}$,¹³ have been prepared. However, the application of the magnetic reagents,

especially in ultra-low temperature, remains a great challenge. The obstacle to the application of the magnetic reagents is mainly attributed to the following two reasons: one is that the magnetic entropy of the magnetic materials synthesized so far is not large enough, leading to a small temperature change in each refrigeration cycle; another is that the thermal conductivity of the magnetic materials synthesized so far is not good enough, decreasing the thermal efficiency of the refrigeration cycle. To our surprise, although great many efforts have been made to investigate the MCE of the materials, the study of their thermal conductivity is seldom recognized.

Gadolinium hydroxides (for an example, $\text{Gd}(\text{OH})_3$), possessing large metal/ligand ratios, are expected to have a large MCE. Theoretical calculation based on $nR \ln(2S + 1)/M_w$ reveals that the MCE ($-\Delta S_m$) of $\text{Gd}(\text{OH})_3$ can be up to $83.01 \text{ J kg}^{-1} \text{ K}^{-1}$.¹⁰ More importantly, gadolinium hydroxides often crystallize in the high symmetric space group ($P6_3/m$),¹⁴ and thus they may have good thermal conductivity, because thermal conductivity of non-metallic compounds is closely related to their structural symmetry.¹⁵ Considering the fact that the magnetic order temperature of gadolinium hydroxides is extremely low,⁶ it is expected that gadolinium hydroxides are good candidates as ultra-low temperature magnetic reagents. Along this line, we, respectively, use Gd_2O_3 and $\text{Gd}(\text{NO}_3)_3$ to synthesize gadolinium hydroxides, and report herein the MCE and thermal conductivity of two gadolinium hydroxides, namely, $\text{Gd}(\text{OH})_3$ (1) and $\text{Gd}_2\text{O}(\text{OH})_4(\text{H}_2\text{O})_2$ (2).

Compound 1 was obtained through hydrothermal reaction of Gd_2O_3 and NaOH ,‡ instead of the previously reported method which requires the dissolution of Gd_2O_3 in HNO_3 .¹⁶ The single-crystal structure of 1 reveals that it crystallizes in the hexagonal space group $P6_3/m$, in accord with previous research by Beall and his co-workers.¹⁴ Each asymmetric unit of 1 consists of $1/6 \text{ Gd}^{3+}$ ion and $1/2 \text{ OH}^-$ ion. Each Gd^{3+} ion coordinated with nine $\mu_3\text{-OH}^-$ groups in tetrakaidecahedron geometry (Fig. 1a), and each OH^- group bridges three Gd^{3+} ions generating a 3D structure with a 1D hexagram channel as shown in Fig. 1b. The bond lengths of Gd–O are in the range from 2.437 to 2.452 Å,

Collaborative Innovation Center of Chemistry for Energy Materials, State Key Laboratory of Physical Chemistry of Solid Surface and Department of Chemistry, College of Chemistry and Chemical Engineering, Xiamen University, Xiamen 361005, China. E-mail: lslong@xmu.edu.cn; Fax: +86-592-218-3047; Tel: +86-592-2189638

† Electronic supplementary information (ESI) available: The 3D structure of 2, the temperature dependence of the magnetic susceptibility, field-dependent magnetization, specific heat capacity, thermal diffusion coefficients for 1 and 2, the calculation of thermal conductivity of 1 at low temperature, and single-crystal X-ray structure determination of 1 and 2. CCDC 1043508 and 1043509. For ESI and crystallographic data in CIF or other electronic format see DOI: 10.1039/c5cc01254f



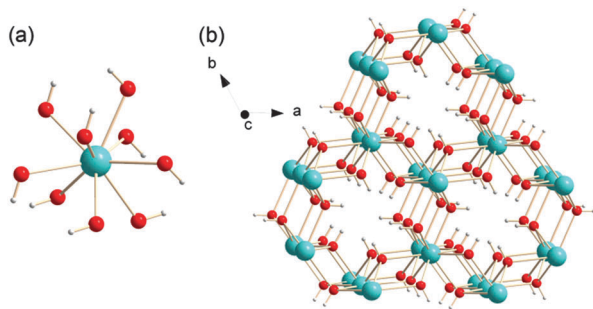


Fig. 1 (a) The coordination environment of Gd^{3+} . (b) The 3D structure of **1**. Gd: cyan, O: red, H: light gray.

the bond angles of Gd-O-Gd are 95.4° to 112.3° , while the separations of $\text{Gd}\cdots\text{Gd}$ are 3.606 \AA and 4.059 \AA respectively.

Compound **2** was obtained through hydrothermal reaction of $\text{Gd}(\text{NO}_3)_3 \cdot 6\text{H}_2\text{O}$, $\text{HCOONa} \cdot 2\text{H}_2\text{O}$ and glycine.[‡] It was mentioned that HCOONa and glycine play an important role in the synthesis. Without HCOONa and glycine, it is impossible to adjust the pH value of the reaction to 6.7. Single-crystal structure analysis reveals that **2** crystallizes in the orthorhombic space group $Cmcm$. The asymmetric unit of **2** consists of 1 Gd^{3+} ion, $1/2 \text{ O}^{2-}$ ion, 2 OH^- ions and one coordination water molecule. There are two crystallography independent Gd^{3+} ions (Gd1 and Gd2) in **2**. The Gd1 is eight-coordinated with six $\mu_3\text{-OH}^-$, one $\mu_3\text{-O}^{2-}$ and one H_2O in dodecahedron geometry, and the Gd2 is nine-coordinated with six $\mu_3\text{-OH}^-$, two $\mu_3\text{-O}^{2-}$ and one H_2O in tetrakaidecahedron geometry. The presence of the O^{2-} in **2** can be demonstrated from its average Gd-O distance and the hydrogen-bonding interaction between the O^{2-} and coordination water molecules, in addition to the charge balance. In **2**, the average Gd-O distance for the O^{2-} is 2.390 \AA , significantly shorter than that of $2.418\text{--}2.5223 \text{ \AA}$ for the OH^- . Consistently, if the $\mu_3\text{-O}^{2-}$ in **2** is taken as $\mu_3\text{-OH}^-$, the hydrogen-bonding interaction between the $\mu_3\text{-OH}^-$ and coordinated water will be unreasonable, because the distance between the H atom in OH^- and the H atom in coordinated water is only about 1.9 \AA .

The 2D structure of **2** can be viewed as connection of adjacent Gd2 ions through two OH^- and one O^{2-} bridges, adjacent Gd1 ions through two OH^- bridges and adjacent Gd1 and Gd2 ions through three OH^- bridges as shown in Fig. 2b. The adjacent

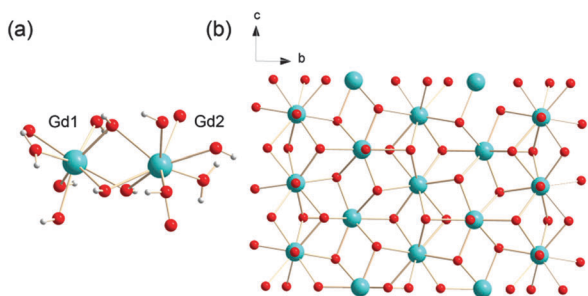


Fig. 2 (a) The coordination environment of Gd^{3+} in **2**. (b) The 2D structure of **2** viewed along the a axis. Gd: cyan, O: red, H: light gray. H atoms in (b) are omitted for clarity.

2D structures connected through hydrogen-bonding interaction between the coordination water molecules from adjacent 2D structures generate a 3D structure of **2** (ESI,[†] Fig. S1). The bond lengths of Gd-O are in the range from 2.324 to 2.617 \AA . The bond angles of Gd-O-Gd are in the range from 93.2 to 111.3° and the $\text{Gd}\cdots\text{Gd}$ separations are in the range from 3.655 to 3.939 \AA . These values are comparable to the corresponding values of **1**.

The temperature dependence of the magnetic susceptibility for **1** and **2** was measured from 2 to 300 K in an applied magnetic field of 1000 Oe respectively. As shown in Fig. S2 (ESI,[†]), the $\chi_{\text{M}}T$ for **1** at 300 K is $8.00 \text{ cm}^3 \text{ K mol}^{-1}$, close to that of $7.88 \text{ cm}^3 \text{ K mol}^{-1}$ calculated for one Gd^{3+} ion ($S = 7/2, g = 2$). The $\chi_{\text{M}}T$ for **2** at 300 K is $15.51 \text{ cm}^3 \text{ K mol}^{-1}$, close to that of $15.75 \text{ cm}^3 \text{ K mol}^{-1}$ calculated for two non-interacting Gd^{3+} ions. With decreasing temperature, the $\chi_{\text{M}}T$ for **1** and **2** remains essentially constant and then decreases gradually from 100 K to 30 K . Upon further lowering the temperature, the $\chi_{\text{M}}T$ drops abruptly, and reaches $3.32 \text{ cm}^3 \text{ K mol}^{-1}$ for **1** and $5.83 \text{ cm}^3 \text{ K mol}^{-1}$ for **2** at 2 K , suggesting the occurrence of antiferromagnetic coupling in **1** and **2**. Consistently, fitting the data in the range of $50\text{--}300 \text{ K}$ with the Curie-Weiss law yields $C = 8.18 \text{ cm}^3 \text{ K mol}^{-1}$, $\theta = -1.69 \text{ K}$ for **1** and $C = 15.84 \text{ cm}^3 \text{ K mol}^{-1}$, $\theta = -4.58 \text{ K}$ for **2**. The overall magnetic coupling characterized by the Weiss constant for **1** and **2** further confirms the occurrence of antiferromagnetic coupling in **1** and **2**.

The measurement of the field-dependent magnetization of **1** and **2** at low temperature ($2\text{--}10 \text{ K}$) was also performed (ESI,[†] Fig. S3). The magnetization of **1** and **2** increases steadily with the applied field and reaches $6.99 N_{\mu_{\text{B}}}$ for **1** and $13.65 N_{\mu_{\text{B}}}$ for **2** at 2 K and 7 T , in agreement with the calculated value of $7 N_{\mu_{\text{B}}}$ for **1** and $14 N_{\mu_{\text{B}}}$ for **2** respectively. Based on these data, the magnetic entropy change, a key parameter in evaluating the MCE, can be obtained by applying the equation of $\Delta S_{\text{m}}(T)_{\Delta H} = \int [\partial M(T, H) / \partial T]_{\text{H}} dH$.¹¹ As shown in Fig. 3, the $-\Delta S_{\text{m}}$ values for **1** and **2** at 2 K and $\Delta H = 7 \text{ T}$ are $62.00 \text{ J kg}^{-1} \text{ K}^{-1}$ ($346.08 \text{ mJ cm}^{-3} \text{ K}^{-1}$) and $59.09 \text{ J kg}^{-1} \text{ K}^{-1}$ ($216.86 \text{ mJ cm}^{-3} \text{ K}^{-1}$) respectively. The $-\Delta S_{\text{m}}$ values for **1** and **2** smaller than the theoretical limiting value of $-\Delta S_{\text{m}} = 83.01 \text{ J kg}^{-1} \text{ K}^{-1}$ ($463.36 \text{ mJ cm}^{-3} \text{ K}^{-1}$) for **1** and $79.57 \text{ J kg}^{-1} \text{ K}^{-1}$ ($292.02 \text{ mJ cm}^{-3} \text{ K}^{-1}$) for **2** calculated by using the equation $-\Delta S_{\text{m}} = nR \ln(2S + 1)/M_{\text{w}}$ are attributed to the occurrence of antiferromagnetic interaction in **1** and **2**.¹⁰ It was mentioned that the gravimetric entropy change larger than $50 \text{ J kg}^{-1} \text{ K}^{-1}$ at 2 K and $\Delta H = 7 \text{ T}$ has only been observed in four compounds (Table 1),^{4,5,17,18} while the volumetric entropy change larger than $210 \text{ mJ cm}^{-3} \text{ K}^{-1}$ has only observed in three compounds so far (including in the commercial magnetic refrigerant GGG^{19}), despite the great many efforts made. Based on Table 1, it is clear that $-\Delta S_{\text{m}}$ for **1** at 2 K and $\Delta H = 7 \text{ T}$ is comparable to that of $66.4 \text{ J kg}^{-1} \text{ K}^{-1}$ ($355 \text{ mJ cm}^{-3} \text{ K}^{-1}$) at 1.8 K and $\Delta H = 7 \text{ T}$, the largest $-\Delta S_{\text{m}}$ reported so far,⁵ while $-\Delta S_{\text{m}}$ for **2** at 2 K and $\Delta H = 7 \text{ T}$ is comparable to that of $55.9 \text{ J kg}^{-1} \text{ K}^{-1}$ ($216 \text{ mJ cm}^{-3} \text{ K}^{-1}$) in $\text{Gd}(\text{HCOO})_3$.⁴

Significantly, MCE for **1** can also reach a satisfying value of $26.9 \text{ J kg}^{-1} \text{ K}^{-1}$ ($150 \text{ mJ cm}^{-3} \text{ K}^{-1}$) at $\Delta H = 2 \text{ T}$. This value is significantly larger than that for GGG ($-\Delta S_{\text{m}} \approx 14.6 \text{ J kg}^{-1} \text{ K}^{-1}$, $105 \text{ mJ cm}^{-3} \text{ K}^{-1}$, at $\Delta H = 2 \text{ T}$),¹⁹ indicating that **1** is a



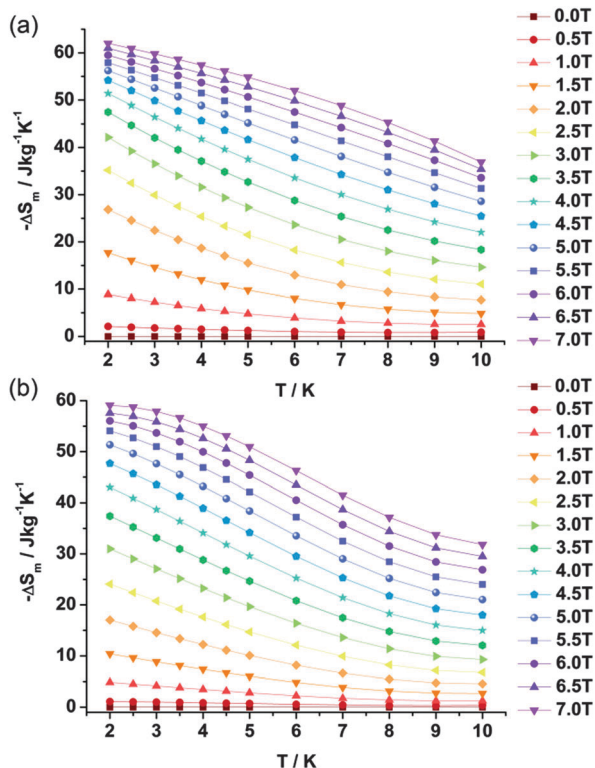


Fig. 3 Values of $-\Delta S_m$ calculated using the magnetization data for **1** (a) and **2** (b) at various fields and temperatures.

Table 1 Magnetic entropy change for selected materials

Compound ^[ref.]	ΔH (T)	$-\Delta S_{m,max}$ (J kg ⁻¹ K ⁻¹)	$-\Delta S_{m,max}$ (mJ cm ⁻³ K ⁻¹)
{[Mn(H ₂ O) ₆] [MnGd-(oda) ₃] ₂ ·6H ₂ O} _n ¹⁷	7	50.1	114
[Gd(HCOO) ₃] _n ⁴	2	12.3	48
[Mn(glc) ₂ (H ₂ O) ₂] ¹⁸	7	60.3	112
[Gd(OH)CO ₃] _n ⁵	2	34.9	65
GdG	7	38.3	273
	2	14.6	105
1 in this work	7	62.0	346
	2	26.9	150
2 in this work	7	59.1	217
	2	17.0	62

promising magnetic refrigeration material. It was mentioned that although the $-\Delta S_m$ value for **1** at 2 K and $\Delta H = 7$ T is comparable to that for **2** at 2 K and $\Delta H = 7$ T, the $-\Delta S_m$ value for **1** at 2 K and $\Delta H = 2$ T is significantly larger than that for **2** ($-\Delta S_m = 17.0$ J kg⁻¹ K⁻¹, 62 mJ cm⁻³ K⁻¹) at 2 K and $\Delta H = 2$ T, revealing that the weaker the antiferromagnetic interaction in the compound, the larger the MCE in low magnetic field.

Because thermal conductivity properties of the materials play a key role in enhancing the thermal efficiency of the refrigeration cycle, the thermal conductivity for **1** and **2** was investigated respectively, so as to evaluate **1** and **2** as magnetic refrigeration materials. Based on the equation $\kappa = \alpha c_p \rho$ for

non-metal materials²⁰ (where α is the thermal diffusion coefficient, c_p is the specific heat capacity, and ρ is the density of the materials), it is clear that thermal conductivity for a given non-metal material is proportional to its thermal diffusion coefficient, specific heat capacity and density respectively. As the density of **1** and **2** could be obtained from their crystal structures, the thermal diffusion coefficient and the specific heat capacity of **1** and **2** were investigated, respectively, in the temperature range from 312 to 352 K, due to equipment limited. As shown in Fig. S4 (ESI[†]), the specific heat capacity for **1** at 312 K is 0.58 J g⁻¹ K⁻¹. With increasing temperature, the specific heat capacity for **1** remains essentially constant and reaches 0.61 J g⁻¹ K⁻¹ at 352 K. In contrast, the specific heat capacity for **2** is significantly affected with temperature, and it changes from 0.53 J g⁻¹ K⁻¹ at 312 K to 0.71 J g⁻¹ K⁻¹ at 352 K.

Fig. S5 (ESI[†]) illustrates the thermal diffusion coefficient for **1** and **2** measured in the temperature range from 312 to 352 K. With the increase of temperature, the thermal diffusion coefficient for **1** decreases gradually, and reaches 0.41 mm² s⁻¹ at 312 K. However, the thermal diffusion coefficient for **2** increases with the decrease of the temperature and reaches 0.14 mm² s⁻¹ at 312 K. The thermal diffusion coefficient for **1** significantly better than that for **2** is attributed to the symmetry in **1** higher than that in **2**.¹⁵

Fig. 4 illustrates temperature-dependent thermal conductivity of **1** and **2**. The thermal conductivity for **1** increases with the decrease of temperature, while this for **2** decreases with the decrease of the temperature in the temperature range from 312 to 352 K. At 312 K, the thermal conductivity for **1** and **2** is 1.32 and 0.27 W M⁻¹ K⁻¹ respectively. It was noted that the thermal conductivity of **1** at 312 K is in the same order of magnitude as that of the GGG (9 W m⁻¹ K⁻¹)¹⁹ at room temperature. Since the $-\Delta S_m$ value and the thermal conductivity of **1** are significantly larger than those of **2**, the thermal conductivity of **1** in the low temperature range was further investigated theoretically according to the reported method,²¹ due to the equipment limited. Based on the specific heat capacity of **1** measured in the temperature range from 100 to 400 K and the low temperature specific heat of **1** in the temperature range from 0.43 to 5.1 K reported previously,⁶ the thermal conductivity of **1** at 0.93 K (the magnetic order temperature of **1**) is about 4.45 W m⁻¹ K⁻¹ (ESI[†]). Although this value is significantly

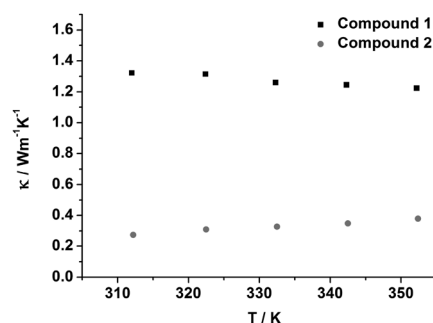


Fig. 4 Temperature-dependent thermal conductivity for **1** and **2**.



smaller than that of about $9 \text{ W m}^{-1} \text{ K}^{-1}$ at 3 K for GGG measured through its single-crystal,²² considering the fact that the thermal conductivity of a given material measured through its powder sample would be significantly smaller than that measured through its single-crystal,²³ it is reasonable to conclude that **1** is a promising candidate for ultra-low temperature magnetic refrigeration material.

In this study, we report the magnetocaloric effect and thermal conductivity of two gadolinium hydroxides, **1** and **2**. The study of their MCE at 2 K and $\Delta H = 2 \text{ T}$ indicates that the $-\Delta S_m$ for **1** is significantly larger than that for **2**, demonstrating that the weaker the antiferromagnetic interaction in the compound, the larger the MCE in low magnetic field. Investigation of their thermal conductivity reveals that the thermal conductivity for **1** is significantly better than that for **2**, revealing that high symmetry of the compound will enhance its thermal conductivity. Considering the fact that MCE for **1** at $\Delta H = 2 \text{ T}$ is significantly larger than that for the GGG and the thermal conductivity of **1** at 0.94 K is up to $4.45 \text{ W m}^{-1} \text{ K}^{-1}$, **1** will be the most promising candidate among the ultra-low temperature magnetic refrigeration reagents reported so far.

This work was supported by the 973 project from MSTC (grant no. 2012CB821704 and 2014CB84561), and the NNSFC (grant no. 21431005 and 21390391).

Notes and references

‡ Synthesis of **1**: Gd_2O_3 (0.363 g, 1 mmol) was dissolved in a freshly prepared aqueous solution of NaOH (10 mL, 20 mol L^{-1}). The resulting mixture was transferred to a Parr Teflon-lined stainless-steel vessel (23 mL). The vessel was heated to 250 °C over a period of 300 min, maintained at that temperature for 4000 min, and then cooled to room temperature. Colourless crystals were obtained in 91.1% yield (based on Gd). C, H, and N analysis (%) calculated for GdH_3O_3 (FW = 208.27) was: C 0, H 1.45, N 0; the experimental analysis was: C 0.041, H 1.52, N 0.043. IR date (KBr , cm^{-1}): 3437 (s), 1630 (w), 1051 (w), 698 (s). Synthesis of **2**: $\text{Gd}(\text{NO}_3)_3 \cdot 6\text{H}_2\text{O}$ (0.113 g, 0.25 mmol), $\text{HCOONa} \cdot 2\text{H}_2\text{O}$ (0.034 g, 0.33 mmol) and glycine (0.006 g, 0.08 mmol) were dissolved in deionized water (15 mL). A freshly prepared aqueous solution of $\text{NH}_3 \cdot \text{H}_2\text{O}$ (1.0 mol L^{-1}) was added dropwise to adjust the pH of the solution to 6.7 while stirring. The resulting mixture was transferred to a Parr Teflon-lined stainless-steel vessel (23 mL). The vessel was heated to 160 °C over a period of 250 min, maintained at that temperature for 4000 min, and then cooled to room temperature over a period of 4000 min. Colourless crystals were obtained in 23.2% yield (based on Gd). C, H, and N analysis (%) calculated for $\text{Gd}_2\text{H}_8\text{O}_7$ (FW = 434.56) was: C 0, H 1.85, N 0; the experimental analysis was: C 0.11, H 1.92, N 0.15. IR date (KBr , cm^{-1}): 3435 (s), 1630 (s), 1383 (s), 1047 (w), 644 (s).

Materials and methods: all reagents and solvents were commercially available and used as received. The C, H and N microanalyses were carried out using a CE instruments EA 1110 elemental analyzer. The infrared spectrum was recorded on a Nicolet AVATAR FT-IR330 spectrophotometer using KBr pellets in the range of 4000–400 cm^{-1} . Magnetic susceptibility was measured using a Quantum Design MPMS superconducting quantum interference device (SQUID). The specific heat

capacity measurement was performed on an NETZSCH DSC 200F3 under a nitrogen atmosphere from 312 K to 352 K with a sweeping rate of 10 K min^{-1} . Thermal conductivity was measured on an NETZSCH LFA457/2/G by a laser flash method under a nitrogen atmosphere in the temperature range of 312–352 K.

- 1 E. Warburg, *Ann. Phys.*, 1881, **249**, 141.
- 2 V. K. Pecharsky and K. A. Gschneidner Jr, *J. Magn. Magn. Mater.*, 1999, **200**, 44.
- 3 (a) J. A. Barclay and W. A. Steyert, *Cryogenics*, 1982, **22**, 73; (b) K. A. Gschneidner Jr and V. K. Pecharsky, *Int. J. Refrig.*, 2008, **31**, 945; (c) B. G. Shen, J. R. Sun, F. X. Hu, H. W. Zhang and Z. H. Cheng, *Adv. Mater.*, 2009, **21**, 4545; (d) Y. Z. Zheng, G. J. Zhou, Z. Zheng and R. E. P. Winpenny, *Chem. Soc. Rev.*, 2014, **43**, 1462; (e) L. Sedláková, J. Hanko, A. Orendáčová, M. Orendáč, C. L. Zhou, W. H. Zhu, B. W. Wang, Z. M. Wang and S. Gao, *J. Alloys Compd.*, 2009, **487**, 425.
- 4 G. Lorusso, J. W. Sharples, E. Palacios, O. Roubeau, E. K. Brechin, R. Sessoli, A. Rossin, F. Tuna, E. J. L. McInnes, D. Collison and M. Evangelisti, *Adv. Mater.*, 2013, **25**, 4653.
- 5 Y. C. Chen, Z. S. Meng, L. Qin, Y. Z. Zheng, J. L. Liu, F. S. Guo, R. Tarasenko, M. Orendáč, J. Prokleška, V. Sechovský and M. L. Tong, *J. Mater. Chem. A*, 2014, **2**, 9851.
- 6 A. T. Skjeltorp, C. A. Catanese, H. E. Meissner and W. P. Wolf, *Phys. Rev. B: Solid State*, 1972, **7**, 2062.
- 7 F. Torres, J. M. Hernández, X. Bohigas and J. Tejada, *Appl. Phys. Lett.*, 2000, **77**, 3248.
- 8 X. X. Zhang, H. L. Wei, Z. Q. Zhang and L. Zhang, *Phys. Rev. Lett.*, 2001, **87**, 157203.
- 9 G. Karotsis, M. Evangelisti, S. J. Dalgarno and E. K. Brechin, *Angew. Chem., Int. Ed.*, 2009, **48**, 9928.
- 10 J. B. Peng, Q. C. Zhang, X. J. Kong, Y. P. Ren, L. S. Long, R. B. Huang, L. S. Zheng and Z. Zheng, *Angew. Chem., Int. Ed.*, 2011, **50**, 10649.
- 11 J. B. Peng, Q. C. Zhang, X. J. Kong, Y. Z. Zheng, Y. P. Ren, L. S. Long, R. B. Huang, L. S. Zheng and Z. Zheng, *J. Am. Chem. Soc.*, 2012, **134**, 3314.
- 12 M. Evangelisti, O. Roubeau, E. Palacios, A. Camón, T. N. Hooper, E. K. Brechin and J. J. Alonso, *Angew. Chem., Int. Ed.*, 2011, **50**, 6606.
- 13 Y. C. Chen, F. S. Guo, Y. Z. Zheng, J. L. Liu, J. D. Leng, R. Tarasenko, M. Orendáč, J. Prokleška, V. Sechovský and M. L. Tong, *Chem. – Eur. J.*, 2013, **19**, 13504.
- 14 G. W. Beall, W. O. Milligan and H. A. Wolcott, *J. Inorg. Nucl. Chem.*, 1977, **39**, 65.
- 15 J. F. Nye, *Physical Properties of Crystals*, Clarendon Press, Oxford, 1957, p. 322.
- 16 S. Mroczkowski, J. Eckert, H. Meissner and J. C. Doran, *J. Cryst. Growth*, 1970, **7**, 333.
- 17 F. S. Guo, Y. C. Chen, J. L. Liu, J. D. Leng, Z. S. Meng, P. Vrabel, M. Orendáč and M. L. Tong, *Chem. Commun.*, 2012, **48**, 12219.
- 18 Y. C. Chen, F. S. Guo, J. L. Liu, J. D. Leng, P. Vrabel, M. Orendáč, J. Prokleška, V. Sechovský and M. L. Tong, *Chem. – Eur. J.*, 2014, **20**, 3029.
- 19 (a) G. A. Sack and D. W. Oliver, *Phys. Rev. B: Solid State*, 1971, **4**, 592; (b) B. Baudun, R. Lagnier and B. Salce, *J. Magn. Magn. Mater.*, 1982, **27**, 315.
- 20 (a) W. J. Parker, R. J. Jenkins, C. P. Butler and G. L. Abbott, *J. Appl. Phys.*, 1961, **32**, 1679; (b) R. Endo, T. Yagi, M. Ueda and M. Susa, *ISIJ Int.*, 2014, **54**, 2084.
- 21 R. Gaumé, B. Viana, D. Vivien, J. Roger and D. Fournier, *Appl. Phys. Lett.*, 2003, **83**, 1355.
- 22 G. A. Slack and D. W. Olivet, *Phys. Rev. B: Solid State*, 1971, **4**, 592.
- 23 J. A. Barclay, S. S. Rosenblum and W. A. Steyert, *Cryogenics*, 1976, **16**, 539; J. A. Barclay, L. Paterson, D. Bingham and O. Moze, *Cryogenics*, 1978, **18**, 535.

